Effect of P microalloying on magnetic properties and structure of FeSiBNbCu nanocrystalline alloy

Changjiu Wang[1,2], Jiawei Li[1,3,*] (iD), Xuhang Zhang[1], Jiaxin Wu[1], Aina He[1,3,*], and Yaqiang Dong[1,3,*]

[1] *CAS Key Laboratory of Magnetic Materials and Devices, and Zhejiang Province Key Laboratory of Magnetic Materials and Application Technology, Ningbo Institute of Materials Technology & Engineering, Chinese Academy of Sciences, Ningbo 315201, Zhejiang, China*

[2] *Nano Science and Technology Institute, University of Science and Technology of China, Suzhou 215123, Jiangsu, China*

[3] *University of Chinese Academy of Sciences, Beijing 100049, China*

ABSTRACT

Phosphorus (P) is a cheap and effective element that inhibits grain growth and improves soft magnetic properties in Fe-based nanocrystalline alloys. However, most alloys usually require high P content, leading to problems such as volatilization and oxidation during production process. In this paper, we study and report new findings regarding the effect of P microalloying on the magnetic properties, microstructure and magnetic domain structure of $Fe_{77.8}Si_{10}B_{9-x}Cu_{0.6}Nb_{2.6}P_x$ ($x = 0$ and 1) nanocrystalline alloys. The substitution of B by 1 at% P has little influence on the crystallization behavior, saturation magnetic flux density (B_s) and permeability (μ) of the alloy, while effectively reduces the coercivity (H_c) in a wide annealing temperature range. The reduced H_c can be attributed to the low magnetocrystalline anisotropy and wide magnetic domains caused by uniform and fine α-Fe(Si) grains. The mechanism of structural evolution induced by 1 at% P is also been discussed. The P microalloyed nanocrystalline alloy with high B_s of 1.43 T, high μ up to 27,000 at 1 kHz, and low H_c of 1.4 A/m is suitable for magnetic shielding piece of wireless charging.

1 Introduction

As consumer electronics industries develop rapidly, there is an increasing need of wireless charging due to their convenient and safe nature [1]. Being one of the key components in wireless charging devices, magnetic shielding pieces can significantly improve charging efficiency by preventing magnetic leakage and reducing electromagnetic eddy current [2–6]. The previous magnetic shielding pieces are made of ferrites or Fe-based amorphous alloys. Nowadays, Fe-based nanocrystalline alloys, especially FeSiBNbCu (Finemet) system, are the preferred materials for wireless charging of consumer electronics due to their high saturation magnetic flux density (B_s), high permeability (μ) and very low core loss at

Address correspondence to E-mail: lijw@nimte.ac.cn; hean@nimte.ac.cn; dongyq@nimte.ac.cn

Springer

100–200 kHz [7–10]. Unfortunately, the typical FeSiBNbCu alloys currently in commercial use cannot meet the development needs of high charging power and thinning at the same time due to its low B_s (< 1.25 T). Therefore, there is an urgent need to develop nanocrystalline alloys with higher B_s and excellent soft magnetic properties for wireless charging.

Most prior research enhanced B_s by increasing the proportion of ferromagnetic elements (such as Fe, Co, etc.) in the composition [11–13]. However, a high proportion of ferromagnetic elements usually reduces the amorphous forming ability (AFA) of the alloys, thereby worsening the soft magnetic properties such as μ and coercivity (H_c) [14]. In addition, expensive Co not only increases the cost of raw materials but also increases the H_c of the alloys, which is not conducive to commercial applications [15]. The addition of early transition metals (especially Nb, Zr, Hf, Ta and Mo) [16–19] was found to impede grain growth to aid in AFA and good soft magnetic properties but at the expense of B_s. Adding a small amount of post-transition metal such as Al could achieve high μ and high B_s but reduced the AFA [20]. Compared with the early transition metals, P with smaller atomic size has less negative influence on B_s, and can effectively improve the AFA and soft magnetic properties of the amorphous and nanocrystalline alloys with high Fe content, while reducing the cost of raw materials [21–23]. For example, the synergy of P, Nb and Cu in FeSiBNbCuP system can improve the initial crystal number density, inhibit the growth of nanocrystals during annealing, and improve the microstructure and soft magnetic properties of the alloys [24]. Substitution of Nb by P can reduce the primary crystallization temperature and improve the μ of FeSiBNbCuP alloys. However, when P was used to completely replace Nb, the optimum annealing temperature range and soft magnetic properties deteriorate [22]. The suitable substitution of P for Si inhibits the precipitation of α-Fe and improves the thermal stability of FeSiBCuCP alloys [21]. In FeSiBCu alloys with high Fe content, replacing B with P expands the optimal annealing temperature range, increases the grain density of nanocrystals, and obtains good soft magnetic properties [25]. In addition, P instead of B substitution can suppress the preferred surface crystallization of FeSiBNbCuP alloys, but excessive P addition would promote the oxidation of Fe [23]. In order to maintain high AFA and good soft magnetic

properties, the above-mentioned alloys usually contain 3 at% or more of P, since a trace amount of P has less effective in preventing grain growth in these alloys. Alloys with high P content are easy to volatilize during smelting process, and are easily oxidized during heat treatment, making them difficult to scale production [23, 26]. Therefore, it is of great significance to develop low-P nanocrystalline alloys with high AFA and excellent soft magnetic properties; and reveal the mechanism of the influence of P microalloying on the structure and magnetic properties of the alloys.

In this work, we study in detail the effect of P microalloying on the magnetic properties and structure of $Fe_{77.8}Si_{10}B_{9-x}Cu_{0.6}Nb_{2.6}P_x$ ($x = 0$ and 1 at%). We find that substituting 1 at% P for B has little effect on B_s and μ, but enabling the achievement of lower H_c. The superior magnetic properties, i.e. high B_s of 1.43 T, high μ up to 27,000 at 1 kHz, and low H_c of 1.4 A/m, make the alloy a good candidate for wireless charging magnetic shields. Trace P addition can not only improve the soft magnetic performance, but also reduce the processing difficulty, which provides ideas for the industrial application of P-containing nanocrystalline alloys. We explore the evolution of magnetic properties caused by the addition of minor P using transmission electron microscopy (TEM), magneto-optical Kerr microscopy and crystallization dynamics analysis.

2 Materials and methods

2.1 Materials

All the raw material utilized in the present work involved high pure Fe (99.99 mass%), Si (99.99 mass%), B (99.95 mass%), Nb (99.99 mass%), Cu (99.99 mass%) and pre-alloyed Fe_3P (99.99 mass%).

2.2 Procedure

Alloy ingots with a composition of $Fe_{77.8}Si_{10}B_{9-x}Cu_{0.6}Nb_{2.6}P_x$ ($x = 0$ and 1) were prepared by induction-melting for three time under purity argon atmosphere. The ingots were then broken into small pieces and put into a quartz tube for vacuum melting. The ribbons with a thickness of 22 μm and a width about 1.1 mm were produced by a single-roller melt-spinning method with copper roller speed of 45 m/s

in an argon atmosphere. The crystallization temperature of the as-quenched ribbons was evaluated by differential scanning calorimetry (DSC, NETZSCH 404C) at a heating rate of 40 K/min under high purity argon flow. Heat treatment of the as-quenched specimens was carried out with a furnace under a vacuum degree of 5×10^{-3} Pa followed by water quenching. The annealing parameters were at 803–883 K for 30 min.

2.3 Physical characterization

The microstructure of the annealed samples was identified by X-ray diffraction (XRD, Bruker D8 Advance) with Cu-Kα radiation and a high-resolution transmission electron microscopy (HRTEM, TF20). The B_s was evaluated through a vibrating sample magnetometer (VSM, Lakeshore 7410) under a maximum applied field of 800 kA/m. The H_c was measured with a DC B-H loop tracer (EXPH-100, Riken Deshi Co., Ltd) under a maximum applied field of 800 A/m. The μ under the frequency range from 1 kHz to 110 MHz was examined by a HP4294A impedance analyzer in a field of 1 A/m. The magnetic domain images were observed by a Magneto-optical Kerr Effect Microscopy using an Evico Magnetics Kerr Microscope (4–873 K/950MT, Germany) in the longitudinal mode. All the measurements were performed at room temperature.

3 Results and discussion

3.1 Thermal properties

The DSC curves of $Fe_{77.8}Si_{10}B_{9-x}Cu_{0.6}Nb_{2.6}P_x$ ($x = 0$ and 1, hereafter labeled as P_0 and P_1, respectively) are shown in Fig. 1. Both the DSC curves of P_0 and P_1 have two distinct exothermic peaks with the onset temperatures marked as T_{x1} and T_{x2}. The T_{x1} of P_0 and P_1 are 750 and 753 K, and the T_{x2} of P_0 and P_1 are 926 and 927 K, respectively. Therefore, the substitution of B by 1 at% P has little effect on the crystallization behavior of the present alloy system. According to previous studies [11], the optimal annealing temperature for the formation of high-density bcc-Fe(Si) nanocrystalline grains that responsible for excellent soft magnetic properties should be between T_{x1} and T_{x2}.

3.2 Magnetic properties

Figure 2 shows the B_s, μ and H_c of P_0 and P_1 as a function of annealing temperature. It is clear that the 1 at% P addition has little influence on the B_s of the alloy within the error range. The slightly decrease in B_s from about 1.45 T for P_0 to about 1.43 T for P_1 is ascribed to the substitution of B by P that has larger atomic size and mass. Although the μ of P_0 is greater than that of P_1 at 803 K, the μ of P_1 increases with the annealing temperature and reaches the maximum value above 27,000 at 833 K, which is greater than the μ of P_0. In a wide annealing temperature range, the substitution of 1 at% P for B has no obvious effect on the μ of the alloy, but it can effectively reduce H_c. As shown in Fig. 2, with the increase of annealing temperature, the H_c of P_0 increases from 2.3 to 3.9 A/m, whereas the H_c of P_1 remains around unchanged and can be as low as 1.4 A/m. The low H_c can reduce the hysteresis loss during high-frequency magnetization [11], which is beneficial to improve the efficiency of wireless charging.

3.3 Microstructure analysis

According to Herzer's random anisotropy model [27], H_c is related to the grain size of nanocrystalline alloys. And the reduction of H_c significantly depends on the magneto-crystalline anisotropy, interparticle interaction and size [28]. In order to clarify the influence of trace P addition on the H_c of the alloy, the microstructure and magnetic domain structure were analyzed by XRD, TEM, and magneto-optic
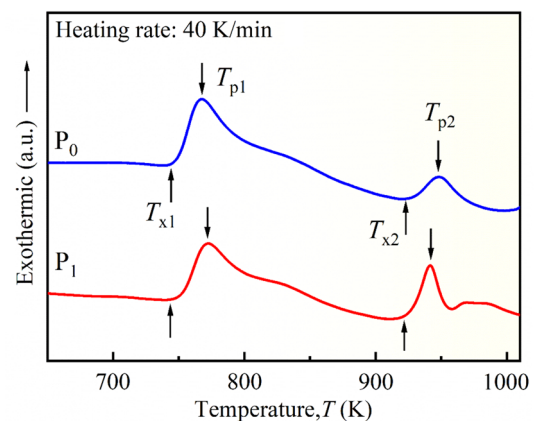

Fig. 1 DSC traces of as-quenched P_0 and P_1 ribbons at a heating rate of 40 K/min. T_{p1} and T_{p2} represent the temperature of the first and second peaks, respectively
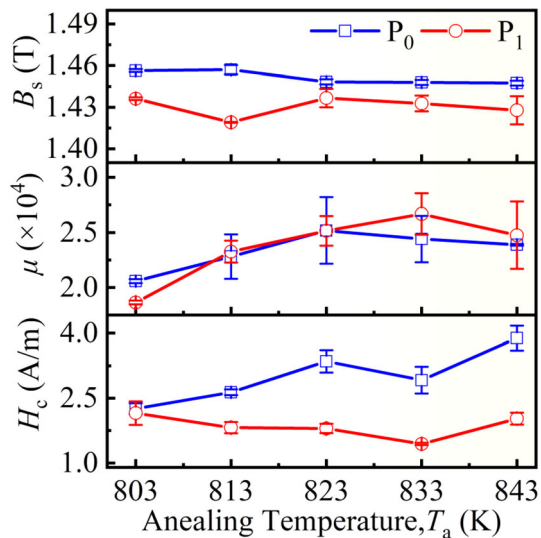
Fig. 2 B_s, μ and H_c of P_0 and P_1 as a function of annealing temperature

Kerr microscope, respectively. Figure 3 displays the XRD patterns of P_0 and P_1 annealed at 803–843 K for 30 min. It is clear that all the samples exhibit one sharp crystalline peak at about $2\theta = 45°$ and two weaker peaks at about $2\theta = 65°$ and $83°$, indicating that only α-Fe(Si) single phase is embedded in the residual amorphous matrix [20]. No Fe-boride phase can be observed. With the increase of annealing temperature, the intensity of the crystallization peaks of P_0 and P_1 increases slightly. Figure 4 depicts the TEM micrographs, selected-area electron diffraction (SAED) images and characteristic grain size distribution of P_0 and P_1 annealed at 803 and 843 K. The SAED patterns with a halo pattern and the typical α-Fe(Si) polycrystalline diffraction ring further prove the coexistence of α-Fe(Si) and amorphous phases [29]. The characteristic distribution and average grain sizes D are shown in the histograms. The grain sizes of P_0 and P_1 are almost the same at 803 K, thus their H_c values are similar. The H_c value of P_0 boosts at 843 K, which results from a grain of the average grain size from 11.69 nm at 803 K to 13.85 nm at 843 K and its wider characteristic distribution. However, 1 at% P effectively prevents the growth of α-Fe(Si) at 843 K, thus the grain size and characteristic distribution of P_1 remain basically unchanged as temperature becomes higher. This enables P_1 to maintain low H_c in a wide annealing temperature range.

Figure 5 shows the magnetic domain structure of the as-quenched and annealed P_0 and P_1. Two kinds of domain structure are observed in the as-quenched
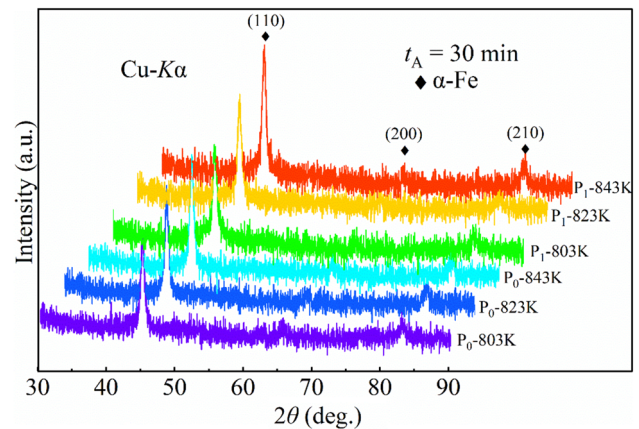

Fig. 3 XRD patterns of P_0 and P_1 at 803, 823, and 843 K

state, (a) and (b), including the curved domains with 180° domain wall and the fingerprint-like maze domains. This domain structure is mainly due to the internal stress induced by fast-quenching, and the narrow maze domains indicate the non-uniformity of the stress [30, 31]. The domain structure of P_0 and P_1 annealed at 843 K contains only 180° linear domains, (c) and (d). This is because the internal stress, magnetocrystalline anisotropy and magnetostriction coefficient of the annealed samples are reduced, resulting in the decrease of effective magnetic anisotropy [27, 32]. Thus, the maze domains disappear, leaving only relatively regular linear domains. In addition, pinning points present in the middle of the domain wall of P_0. Conversely, P_1 has a wider and better arrangement domain wall than P_0, which can be attributed to the reduced magnetic crystal anisotropy resulted from its finer and more uniform α-Fe(Si) nanocrystalline grains. This points to a smaller resistance of the magnetic domain movement of P_1 when compared to P_0; and a smaller H_c in a wide annealing temperature range.

3.4 Crystallization dynamics analysis

To provide further evidence that trace P addition can effectively refine the grains of the FeSiBCuNb alloy, we performed crystallization thermodynamic analysis via measuring the DSC curves of P_0 and P_1 with heating rates of 5, 10, 20 and 40 K/min. The results are substituted into Kissinger equation [33], and the activation energies. The latter is estimated from the onset of crystallization temperature and the peak temperature, marked as E_{x1} and E_{P1}, respectively. The Kissinger equation is as follows:
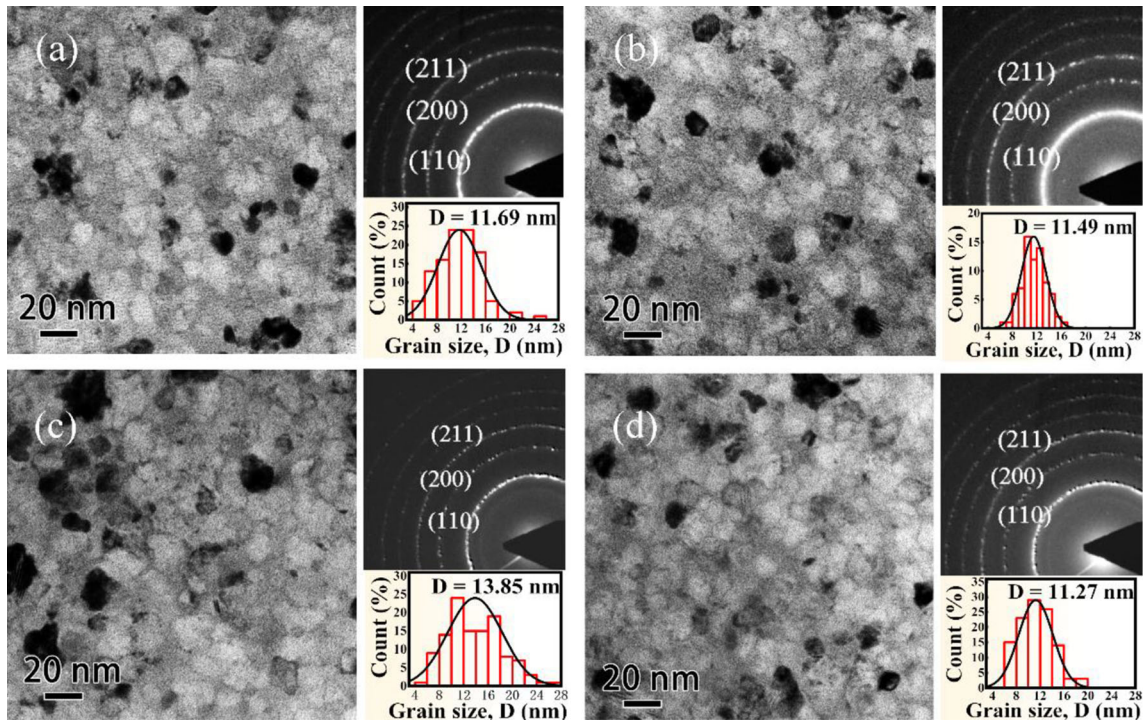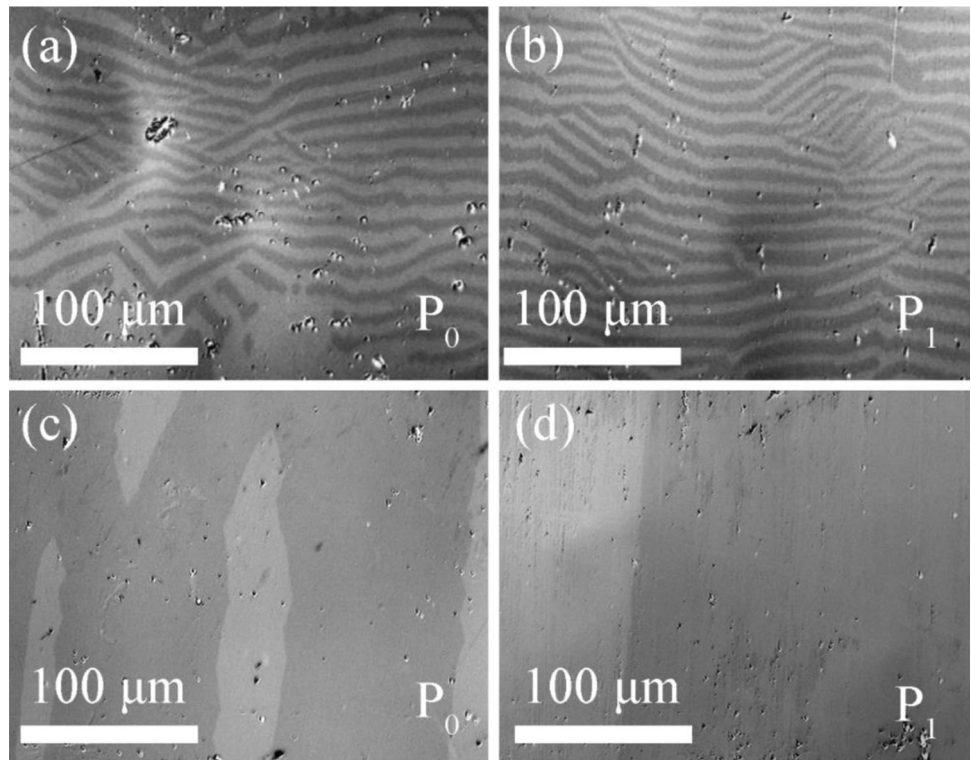
Fig. 4 TEM micrographs, SAED images and characteristic grain size distribution of **a** P_0 at 803 K, **b** P_1 at 803 K, **c** P_0 at 843 K, and **d** P_1 at 843 K

Fig. 5 Magnetic domain structure of P_0 and P_1. **a** and **b** as-quenched; **c** and **d** annealing at 843 K for 30 min

$$\ln\left(\frac{T_p^2}{\beta}\right) = \frac{E_p}{RT_p} + \text{const}, \qquad (1)$$

where β is the heating rate, T_p is the crystallization peak temperature at a specific heating rate, R is the perfect gas constant (8.314472 J/mol/K), and E_p is the activation energy of crystallization.

The corresponding Kissinger plot and the specific activation energy of crystallization are shown in Fig. 6. The slope of the fitted curve in Fig. 6a represents the magnitude of the crystallization activation energy. The greater the slope, the greater the activation energy. It can be seen from Fig. 6a that the slope of the fitted curve of P_1 is larger. The E_{x1} values of P_0 and P_1 are greater than the E_{p1} values of P_0 and P_1 (see Fig. 6b), meaning that the nuclear process requires less energy than the growth process. Thus the growth process may occur more frequently than the nucleus process. The E_{x1} and E_{p1} of P_0 are 326 and 308 kJ/mol, respectively. With the addition of 1 at% P, the E_{x1} and E_{p1} of P_1 are increased to 402 kJ/mol and 370 kJ/mol, respectively. Therefore, P_1 requires higher activation energy for nucleation and growth than P_0, indicating that the nucleation and growth of α-Fe(Si) in P_1 are inhibited effectively. This is consistent with the results of TEM and magneto-optic Kerr microscope.

4 Conclusion

The effect of P microalloying on the magnetic properties and structure of $Fe_{77.8}Si_{10}B_{9-x}Cu_{0.6}Nb_{2.6}P_x$ ($x = 0$ and 1 at%) nanocrystalline alloy has been studied. The substitution of 1 at% P for B has almost no effect on the B_s and μ of the alloy, but the H_c is effectively decreased and stabilized in a wide annealing temperature range. The analysis of crystallization kinetics shows that the addition of 1 at% P can significantly inhibit the nucleation and growth of crystal grains, thus the P microalloyed alloy can form more uniform and finer α-Fe(Si) grains. This benefits the alloy to obtain low magnetocrystalline anisotropy and wide magnetic domains, and excellent soft magnetic properties, i.e. high B_s of 1.43 T, high μ up to 27,000 at 1 kHz, and low H_c of 1.4 A/m. This work provides a design strategy for low-P nanocrystalline alloys with high AFA and excellent soft magnetic properties.

Compliance with ethical standards

Conflict of interest The authors declare no conflict of interest.

Fig. 6 **a** Kissinger plots and **b** crystallization activation energy of P_0 and P_1
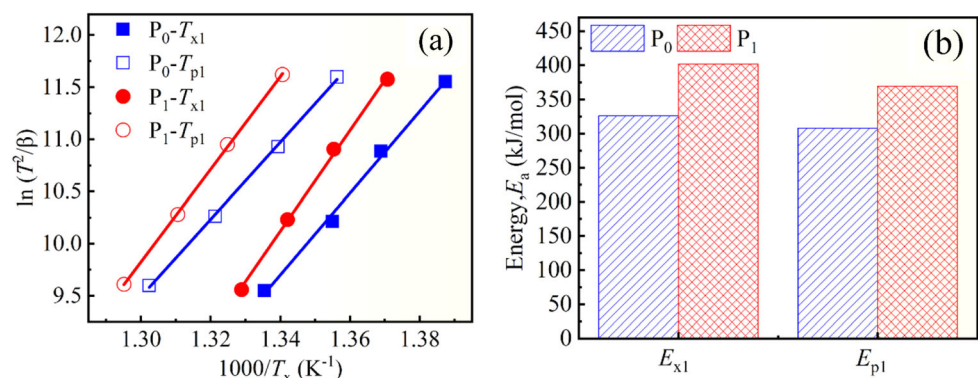
References

1. H. Dai, Y. Liu, G. Chen, X. Wu, T. He, A.X. Liu, H. Ma, Safe charging for wireless power transfer. IEEE ACM Trans. Netw. **25**(6), 3531–3544 (2017)

2. I.G. Lee, N. Kim, I.K. Cho, I.P. Hong, Design of a patterned soft magnetic structure to reduce magnetic flux leakage of magnetic induction wireless power transfer systems. IEEE Trans. Electromagn. Compat. **59**(6), 1856–1863 (2017)

3. Z. Dai, J. Wang, M. Long, H. Huang, M. Sun, Magnetic shielding structure optimization design for wireless power transmission coil. AIP Adv. **7**(9), 095013 (2017)

4. S. Morita, T. Hirata, E. Setiawan, I. Hodaka, *IEEE, Power Efficiency Improvement of Wireless Power Transfer Using Magnetic Material* (Shenzhen, IEEE, 2017), pp. 304–307

5. D. Azuma, N. Ito, M. Ohta, Recent progress in Fe-based amorphous and nanocrystalline soft magnetic materials. J. Magn. Magn. Mater. **501**, 166373 (2019)

6. A. Krings, A. Boglietti, A. Cavagnino, S. Sprague, Soft magnetic material status and trends in electric machines. IEEE Trans. Ind. Electron. **64**(3), 2405–2414 (2017)

7. Y. Yoshizawa, S. Oguma, K. Yamauchi, New Fe-based soft magnetic alloys composed of ultrafine grain structure. J. Appl. Phys. **64**(10), 6044–6046 (1988)

8. T. Luo, J. Xu, G. Wang, W. Cai, Y. Yang, Composition dependence of amorphous forming, crystallization behavior, magnetic and electronic properties of silicon-rich FeSiBCuNb alloys. J. Magn. Magn. Mater. **505**, 166714 (2020)

9. X. Wu, X. Li, S. Li, Crystallization kinetics and soft magnetic properties of $Fe_{71}Si_{16}B_9Cu_1Nb_3$ amorphous alloys. Mater. Res. Express. **7**(1), 1–7 (2020)

10. Y. Wang, Y. Tian, T. Kirk, O. Laris, J.H. Ross, R.D. Noebe, V. Keylin, R. Arróyave, Accelerated design of Fe-based soft magnetic materials using machine learning and stochastic optimization. Acta Mater. **194**, 144–155 (2020)

11. M.A. Willard, M. Daniil, Nanocrystalline soft magnetic alloys two decades of progress. Handb. Magn. Mater. **21**, 173–342 (2013)

12. R. Parsons, B. Zang, K. Onodera, H. Kishimoto, A. Kato, K. Suzuki, Soft magnetic properties of rapidly-annealed nanocrystalline Fe-Nb-B-(Cu) alloys. J. Alloys Compd. **723**, 408–417 (2017)

13. P.B. Liu, S. Gao, Y. Wang, Y. Huang, F.T. Zhou, P.Z. Liu, Magnetic porous N-doped carbon composites with adjusted composition and porous microstructure for lightweight microwave absorbers. Carbon **173**, 655–666 (2021)

14. L. Shi, K. Yao, Composition design for Fe-based soft magnetic amorphous and nanocrystalline alloys with high Fe content. Mater. Des. **189**, 108511 (2020)

15. M. Kuhnt, X.D. Xu, M. Amalraj, P. Kozikowski, K.G. Pradeep, T. Ohkubo, M. Marsilius, T. Strache, C. Polak, M. Ohnuma, K. Hono, G. Herzer, The effect of Co addition on magnetic and structural properties of nanocrystalline (Fe, Co)-Si-B-P-Cu alloys. J. Alloys Compd. **766**, 686–693 (2018)

16. X. Jia, Y. Li, G. Xie, T. Qi, W. Zhang, Role of Mo addition on structure and magnetic properties of the $Fe_{85}Si_2B_8P_4Cu_1$ nanocrystalline alloy. J. Non Cryst. Solids **481**, 590–593 (2018)

17. J.F. Li, X. Liu, S.F. Zhao, H.Y. Ding, K.F. Yao, Fe-based bulk amorphous alloys with iron contents as high as 82 at%. J. Magn. Magn. Mater. **386**, 107–110 (2015)

18. C. Suryanarayana, A. Inoue, Iron-based bulk metallic glasses. Int. Mater. Rev. **58**(3), 131–166 (2013)

19. K. Suzuki, A. Makino, N. Kataoka, A. Inoue, T. Masumoto, High saturation magnetization and soft magnetic properties of bcc Fe–Zr–B and Fe–Zr–B–M (M = Transition metal) alloys with nanoscale grain size. Mater. Trans. **32**(1), 93–102 (1991)

20. J. Wu, A. He, Y. Dong, J. Li, Y. Lu, Structural and magnetic characterization of Al microalloying nanocrystalline FeSiBNbCu alloys. J. Magn. Magn. Mater. **505**, 166746 (2020)

21. J. Xu, Y. Yang, Q. Yan, F. Hou, C. Fan, G. Wang, T. Luo, Effects of the substitution of Si by P on crystallization behavior, soft magnetic properties and bending ductility of FeSiBCuPC alloys. J. Alloys Compd. **816**, 152534 (2019)

22. Y.R. Jia, Z. Wang, F. Wang, Y. Han, Z.Y. Xie, L.J. Li, L. Zhang, Effect of P substitution for Nb on structure and soft magnetic properties of Si-rich FeCuNbSiB nanocrystalline alloys. Mater. Sci. Eng. B **222**, 55–59 (2017)

23. B. Butvinova, P. Butvin, K. Brozka, M. Kuzminski, I. Mat'ko, P. Svec, M. Chromcikova, Effects of surface crystallization and oxidation in nanocrystalline FeNbCuSiB(P) ribbons. J. Magn. Magn. Mater. **424**, 233–237 (2017)

24. Z. Li, A. Wang, C. Chang, Y. Wang, B. Dong, S. Zhou, Synthesis of FeSiBPNbCu nanocrystalline soft-magnetic alloys with high saturation magnetization. J. Alloys Compd. **611**, 197–201 (2014)

25. A.D. Wang, H. Men, B.L. Shen, G.Q. Xie, A. Makino, A. Inoue, Effect of P on crystallization behavior and soft-magnetic properties of $Fe_{83.3}Si_4Cu_{0.7}B_{12-x}P_x$ nanocrystalline soft-magnetic alloys. Thin Solid Films **519**(23), 8283–8286 (2011)

26. C.J. Wang, A.N. He, A.D. Wang, J. Pang, X.F. Liang, Q.F. Li, C.T. Chang, K.Q. Qiu, X.M. Wang, Effect of P on glass forming ability, magnetic properties and oxidation behavior of FeSiBP amorphous alloys. Intermetallics **84**, 142–147 (2017)

27. G. Herzer, Modern soft magnets: amorphous and nanocrystalline materials. Acta Mater. **61**(3), 718–734 (2013)

28. A. Turky, M. Rashad, A. Hassan, E. Elnaggar, M. Bechelany, Tailoring optical, magnetic and electric behavior of lanthanum strontium manganite La1xSrxMnO3 (LSM) nanopowders prepared via a co-precipitation method with different Sr2+ ion contents. RSC Adv. **6**, 17980 (2016)

29. R.K. Roy, A.K. Panda, A. Mitra, Effect of Co content on structure and magnetic behaviors of high induction Fe-based amorphous alloys. J. Magn. Magn. Mater. **418**, 236–241 (2016)

30. P.B. Chen, A.D. Wang, C.L. Zhao, A.N. He, G. Wang, C.T. Chang, X.M. Wang, C.T. Liu, Development of soft magnetic amorphous alloys with distinctly high Fe content. SCI China Phys. Mech. **60**(10), 106111 (2017)

31. M. Tejedor, J.A. García, J. Carrizo, L. Elbaile, Mechanical determination of internal stresses in as-quenched magnetic amorphous metallic ribbons. J. Mater. Sci. **32**(9), 2337–2340 (1997)

32. S. Flohrer, R. Schäfer, C. Polak, G. Herzer, Interplay of uniform and random anisotropy in nanocrystalline soft magnetic alloys. Acta Mater. **53**(10), 2937–2942 (2005)

33. R.L. Blaine, H.E. Kissinger, Homer kissinger and the kissinger equation. Thermochim Acta **540**, 1–6 (2012)

Publisher's Note Springer Nature remains neutral with regard to jurisdictional claims in published maps and institutional affiliations.